3

Robotic Applications of Artificial Muscle Actuators

H.R. Choi[1], K.M. Jung[2], J.C. Koo[2], J.D. Nam[3]

[1] School of Mechanical Engineering, College of Engineering,
Sungkyunkwan University, Suwon 440-746, Korea
hrchoi@me.skku.ac.kr
[2] School of Mechanical Engineering, College of Engineering,
Sungkyunkwan University, Suwon 440-746, Korea
jungkmok@me.skku.ac.kr
[3] School of Mechanical Engineering, College of Engineering,
Sungkyunkwan University, Suwon 440-746, Korea
jckoo@me.skku.ac.kr
[4] Department of Polymer Science and Engineering, College of Engineering
Sungkyunkwan University, Suwon 440-746, Korea
jdnam@skku.edu

3.1 Introduction

For the last few decades, the roles of robots have been widely expanded from handling of routine manufacturing processes to hosting various entertainment applications. With the evolution of the information technology that creates ubiquitous communication environments in human life, the expectation of advances in robotic technology has been more intensified. Obviously, development of new robot applications has outpaced the improvement of mechanical and electrical functionality of robot hardware. One of the most languid activities in the hardware development in robotics might exist in the field of sensors and actuators. For instance, the efficacy of control algorithms or information handling of the current cutting-edge robots is often constrained by actuator performance, sensing capabilities, mechanical locomotion, or power sources.

According to the development trends of robots, their functionality is recently concentrated on mimicking human movements or animal functions. Introduction of new kinds of actuators, so-called *soft* actuators, might be of key interest in the new robot technology development. However, the physical properties of traditional transducers such as electromagnetic motors, voice coil motors, are truly different from that of animal muscles so that operation of a robot equipped with actuators should be confined and efficient only in a structured environment. As a result, providing some level of flexibility to a robot skeleton and also to actuators will be the critical development path of the next generation of robots.

Energy transduction considered from the thermodynamic point of view does not provide ample research opportunities mainly because the macroscopic

observation of energy flow has been well characterized. Especially energy flow in mechanical-electrical domain energy transformation that most likely relies on electromagnetic phenomena has been scrutinized for some decades. Consequently, most of the engineering applications, where the mechanical-electrical energy transformation is needed, employ electromagnetic transducers. Material development for energy transduction is, however, in its infancy. Recognizing the available number of transducer types that could be adopted in mechanical-electrical domain energy transformation, the development of an innovative new energy transformation material is well motivated.

Despite the tremendous engineering research opportunities in the development of *soft* actuators for robotic applications, this field of study has been in a lukewarm stage for years. The advent of EAPs (electroactive polymers) recently constitutes an enormous impact on lingering development activity. There are a couple of reasons why the materials deserve keen attention from the robotic engineering field. First, they could provide rectilinear motions without any assistance from a complicated power train. Recognizing that a complicated power transfer mechanism creates bulky robots and it hampers accomplishing delicate missions, total elimination or partial reduction of the power train mechanism benefits expansion of robot application where precise operation is required. Besides, reducing the number of power transmission stages, of course, improves energy efficiency. Second, the inherent flexibility of polymeric materials offers many engineering possibilities for creating biomimetic machines. Acknowledging the fact that animals are naturally soft, more precisely their actuation devices are soft, development of the soft energy transducer should be one of the most important prerequisites for biomimetic robot operations [1, 2].

Although actuators made with the polymers seem to provide many advantages over the traditional electromagnetic actuators, there are still some controversies over the feasibility of actuators. Stability and durability issues of the material, when it is manufactured as an actuator, are the principal concerns of the contention. However, considering the development progress that remains at a primitive stage and the lack of refined manufacturing technology, the debate might not be the limitation or failure of the technology but the consequences for improvement. There are many different polymeric materials available for development, and the research on the polymer transducers is truly multidisciplinary. Especially when a multidisciplinary technology is in its infancy, typically no dominant solution or consensus can be easily made to concentrate resources and accelerate research activities. Despite the ongoing arguments, the prominent beneficiary of polymer actuator technology might be the field of robotics. There are a number of books and articles available on polymer sensors and actuators. Most of them deliver quite a broad range of information about energy transformation from the basic principles to advanced physical phenomena. However, this chapter departs from the norm. In this chapter, robotic devices made with the polymer, especially dielectric elastomer, are introduced. All devices are successfully controlled with the standard feedback or feedforward algorithms. Focusing on robotic applications by coupling polymeric physics and robotic devices, this chapter would be a valuable asset and also an arsenal for readers to explain emerging robotic actuator technology.

There are various types of EAPs available for actuator development, and they are categorized in two groups by energy transduction characteristics. Ionic and nonionic are the groups of materials. Dielectric elastomers are a sort of non-ionic material. In addition, they are normally incompressible but highly resilient so that a high strain level can be achieved. Silicone and acrylic materials are typical examples of dielectric elastomers. An actuator made with dielectric material is basically a two-plate capacitor. A laminated dielectric elastomer sheet is coated with compliant electrodes on both sides. When an electrical field is applied across the electrodes, positive and negative charges are accumulated near the electrode. This generates coulombic attraction forces between the electrodes, and it results in mechanical pressure, called Maxwell stress. Compressive mechanical pressure moves the electrodes closer to each other. Consequently, the incompressible elastomer expands in lateral directions and yields displacement [3].

Although a wide range of active researches has been undertaken for the improvement of many different EAPs, emphases on dielectric elastomer actuators are made in this chapter because the materials are currently more popularly applied to industrial applications than the other EAPs. Two distinct implementations of the material to robotic actuation are introduced. The construction and functionality of the polymer actuators are closely dependent on the initial stretching of the material, so the design concepts and fabrication of polymer actuators with prestrain are provided and followed by those without prestrain.

3.2 Prestrained Dielectic Elastomer Actuator

3.2.1 Fundamentals of Prestrained Actuator

The basic operation of the dielectric elastomer actuator is simply that the polymer intrinsically deforms either in expanding or in contracting when electrical voltage is applied to the electrodes. Basic principle actuation mechanisms are well explained in many publications [4-6]. Although numerous authors recently have presented various polymer actuators, few have demonstrated practical feasibility of designs and controllable actuator systems that can be implemented with a reasonable amount of control action. In this section, an antagonistically configured dielectric elastomer actuator is presented. Given the material and the geometrical constraints which should be well accounted in controllable actuation, it successfully delivers controlled bidirectional rectilinear mechanical motions by changing its compliance and exerting force.

The principal operation is similar to the electromechanical transduction of a parallel two-plate capacitor, as shown in Figure 3.1. When an electric potential is applied across the polymer film coated with compliant electrodes on both sides, the material is compressed in thickness and expands in the lateral direction. By virtue of this contraction, mechanical actuation force is generated. This physics couples mechanical and electrical energy domains so that energy transduction happens. The effective mechanical pressure, called Maxwell stress along the thickness direction by electrical input, is given by

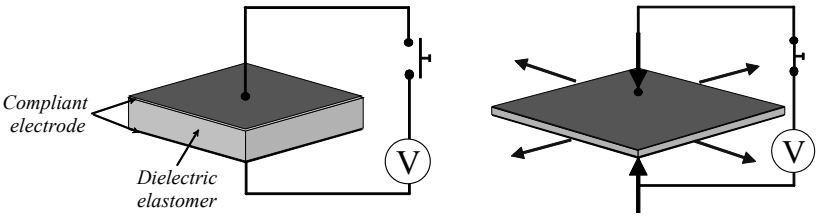

(a) voltage off (b) voltage on

Figure 3.1. Basic actuation mode of a dielectric elastomer actuator

$$\sigma_e = -\varepsilon_o \varepsilon_r E^2 \tag{3.1}$$

where E is an applied electric field, and ε_o and ε_r are the electric permittivity of free space and the relative permittivity, respectively.

Although the way to acquire mechanical actuation from the basic dielectric elastomer is straightforward, there is still a significant limitation for the basic actuation to be used for a practical application mainly due to its low exerting forces. It is simply because the actuation is provided by a soft and thin polymer film. In addition, the thin polymer film used for the basic operation can be easily ruptured by even small normal forces or buckled by lateral forces. Moreover, the operation is hardly controlled so that it is practically called a simple movement rather than an actuation. One of the possible solutions to overcome the critical limitation of the basic actuation mechanism is prestrained actuator design. This concept was originally proposed by researchers in SRI and they demonstrated a 100% length change of a dielectric polymer sheet by applying pretension in the actuation direction [5].

3.2.2 Antagonistic Configuration of a Prestrained Actuator

Noting the fundamental limitations of the basic actuation mechanism, a novel design of an antagonistically configured actuation mechanism, called ANTLA (antagonistically driven linear actuator) is introduced. A schematic illustration of the mechanism is provided in Figure 3.2. With the prestrain effect of the configuration, a polymer sheet may produce a relatively larger displacement [4], although a recent study proves that it is not necessary for acquiring a large strain [6]. Having the prestrained polymer sheet connected to both frame and output terminal, a combination of push-pull forces produces larger actuation displacements.

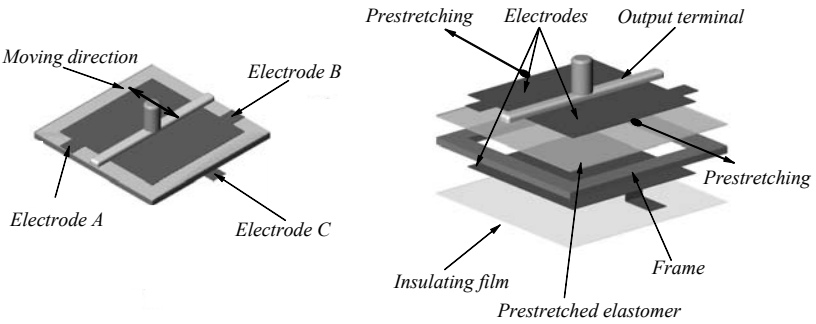

Figure 3.2. Fabrication of antagonistically driven actuator

In this design, the actuator is actually composed of a single prestretched elastomer film affixed to a rigid square frame, which provides uniform pretension in the direction of actuation. For the antagonistically driven mechanism that requires two independent polymer sections, a polymer sheet is stretched and a compliant electrode paste is placed on the top and bottom surfaces. Finally, the top compliant electrode is partitioned in two sections. They are called electrode A and B of the top surface, and the common electrode C of the bottom in Figure 3.2. In addition, a mechanical output terminal is attached at the boundary of the partitioned electrodes. Although it is fabricated from a single elastomer film, it works as the antagonistically driven actuator with partitioned electrodes so that it can provide bidirectional "push-pull" actuation.

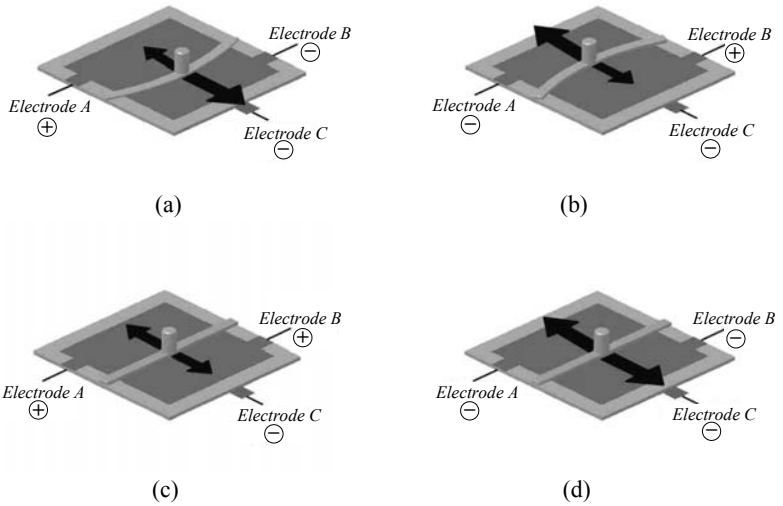

Figure 3.3. Operation

In detail, the device presented works as follows. Assuming that uniform pretensions are engaged, tensions on both sides of the elastomer film are initially balanced. When the electrical input is applied to one of the elastomers, it expands, and the force equilibrium is broken. The output terminal, therefore, moves to rebalance the broken elastic equilibrium. For example, as shown in Figure 3.3a, if a positive input voltage is given on electrode A, a negative one on B, and a negative one on C, then the output terminal moves toward electrode B because the elastomer on electrode A expands due to the input voltage on A. Similarly, if a positive voltage input is given on electrode B while a negative input is applied to A and C, then the output terminal moves toward electrode A. Besides the basic actuation, the design presented can provide an additional feature that is normally difficult to acquire from existing traditional actuators. The compliance of the actuator can be actively modulated by controlling input voltages. For instance, as shown in Figure 3.3c, if positive input voltages are given on electrodes A and B while applying negative voltage to C, the actuator becomes more compliant. On the contrary, it becomes stiffer when all applied voltages are the same. The actuator presented delivers four different actuation states; forward, backward, compliant and stiff, which are characteristics of human muscles.

3.2.3 Modeling and Analysis

3.2.3.1 Static Model

In this section, a static model of the actuator presented is discussed. The modeling process starts from longitudinally dividing the actuator into two sections, as shown in Figure 3.4.

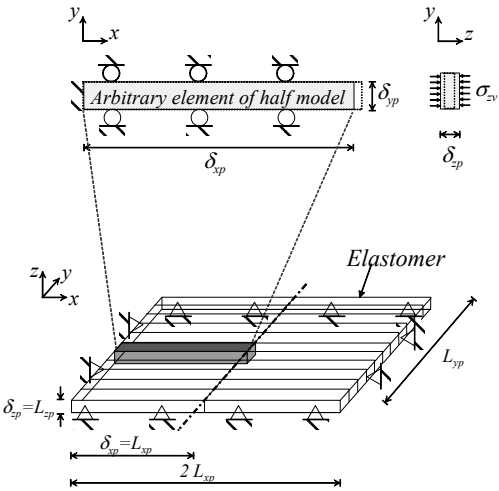

Figure 3.4. Discretization of a polymer sheet

It is then horizontally discretized into a number of elements with infinitesimal width. Then a force balance on an element can be derived, as shown in Figure 3.5. Initially, both the left and right sections of the dielectric elastomer sheet are in elastic force balance.

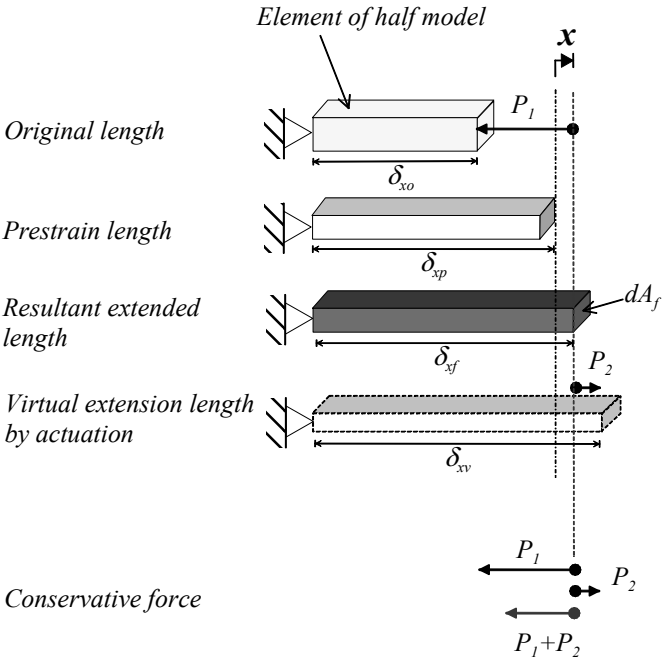

Figure 3.5. Force balance of an element

When electric voltage is applied to one of the sections of the dielectric elastomer, the force equilibrium is rebalanced due to the induced Maxwell stress, noted as P_1 in the figure. The forces P_1 and P_2 can be derived as

$$P_1 = -dA_f Y_x^o \varepsilon_{xp} + \frac{x}{\delta_{xo}} \overset{\Delta}{=} f_1(x)$$

$$P_2 = dA_f Y_x \left(\frac{\delta_{xf}}{\delta_{xo}}\right) \left[\frac{Y_z}{Y_z - \varepsilon_r \varepsilon_o \left(\delta_{zo}/\delta_{zf}\right)\left(V/\delta_{zf}\right)^2} - 1\right] \overset{\Delta}{=} f_2(x, V) \tag{3.2}$$

where the super or subscripts, o, p, and f denote the original unstretched, pre-stretched, and actuated states, respectively. Y_x denotes the x-directional effective elastic modulus, $\circ\varepsilon_{xp}$ stands for x-directional strain caused by prestretching, dA_f is

the cross-sectional area of an element, and ε_o and ε_r denote the permittivity of free space and the relative permittivity of the elastomer, respectively. $f_1(x)$ represents an elastic restoration force caused by prestretching, whereas $f_2(x,V)$ represents an electrostatic force as a function of the displacement x and the applied voltage V. Consequently, the resultant force on the strip is obtained by the summation of the restoration force caused by prestretching and the induced electrostatic force that can be given as

$$P = -Y_x \delta_{yp} \delta_{zf} \left({}^{o}\varepsilon_{xp} + \frac{x}{\delta_{xo}} - \frac{\delta_{xf}}{\delta_{xo}} \right) \left[\frac{Y_z}{Y_z - \varepsilon_r \varepsilon_o \left(\delta_{zo} \big/ \delta_{zf} \right) \left(V \big/ \delta_{zf} \right)^2} + 1 \right] \tag{3.3}$$

where δ_{yp} is the width of the infinitesimal strip of the actuator, as shown in Figure 3.5. The equations obtained from the half strip with infinitesimal width can be easily extended to the full model by integrating the forces from numerous strips with infinitesimal width. In the full model, the final displacement is determined at the equilibrium point between the force of the left half model and that of the right half one, as shown in Figure 3.5. Assuming that the positive direction is toward the right side, in an arbitrary displacement x, the total output force can be derived as

$$F = P_R - P_L \overset{\Delta}{=} g_k \cdot K(x) - g_e \cdot E(x, V_L, V_R) \tag{3.4}$$

where the forces on the output terminal by the left elastomer and the right one are represented by P_L and P_R, $K(x)$ and $E(x,V_L,V_R)$ represent the force by the prestrain and electrostatic effect, and V_L and V_R are input voltages on the left and right sides of the elastomer in Figure 3.4, respectively. $K(x)$ and $E(x,V_L,V_R)$ are defined as

$$K(x) \overset{\Delta}{=} Y_x L_{yp} \left[{}^{o}\varepsilon_{xp} \left(\delta_{Lzf} - \delta_{Rzf} \right) + \frac{x\left(1 + {}^{o}\varepsilon_{xp}\right)}{\delta_{xp}} \left(\delta_{Lzf} + \delta_{Rzf} \right) \right] \tag{3.5}$$

and

$$E(x, V_L, V_R) \overset{\Delta}{=}$$

$$Y_x L_{yp}\left\{\delta_{Lzf}\frac{\delta_{Lxf}}{\delta_{Lxo}}\left[\frac{Y_Z}{Y_Z-\frac{\delta_{Lzo}}{\delta_{Lzf}}\varepsilon_r\varepsilon_o\left(\frac{V_L}{\delta_{Lzf}}\right)^2}-1\right]\right.$$
$$\left.-\delta_{Rzf}\frac{\delta_{Rxf}}{\delta_{Rxo}}\left[\frac{Y_Z}{Y_Z-\frac{\delta_{Rzo}}{\delta_{Rzf}}\varepsilon_r\varepsilon_o\left(\frac{V_R}{\delta_{Rzf}}\right)^2}-1\right]\right\} \tag{3.6}$$

where δ_{Ljf} and δ_{Rjf} are the j directional final length of the left side and the right side. δ_{Ljo} and δ_{Rjo} are the j directional original length of the left and the right sides such as $j = x, z$, respectively, and g_k and g_e are called *effective restoration* and *electrostatic coefficients*, respectively. These coefficients are dependent on geometries such as frame size and thickness of the output terminals. They are determined experimentally in general although they have unit value in the ideal case. Eqs. (3.5) and (3.6) provide the static relations between the displacement and input voltages.

3.2.3.2 Dynamic Model

To derive a dynamic model the actuator presented is simplified as a lumped model , as shown in Figure 3.6. Nevertheless, the mathematical model still has a complicated form because the model has some nonlinear aspects like viscous damping. Based on the lumped model, the dynamic equation of the actuator can be expressed as

$$F(t) = M\ \ddot{x} + B(\dot{x}) + g_k K(x) - g_e E(x, V_L, V_R) \tag{3.7}$$

where $M\ddot{x}$ is the inertial force, $B(\dot{x})$ represents the damping force, and $F(t)$ denotes external forces. $K(x)$ and $E(x, V_L, V_R)$ are obtained from Eqs. (3.5) and (3.6), and the other terms, $M\ \ddot{x}$ and $B(\dot{x})$, are to be derived next. M is the summation of the mass of the load, structural parts, and elastomer film of the actuator, and it varies during operation.

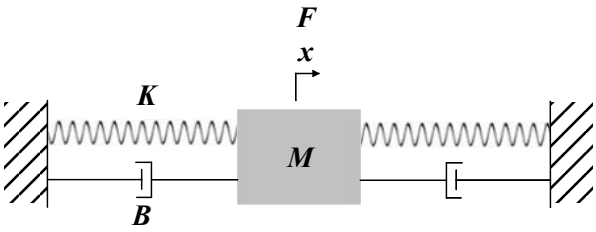

Figure 3.6. Dynamic model of the actuator

In the present formulation, however, only the equivalent mass of the elastomer is considered, and the other terms such as the mass of the output terminal may be included in the model by increasing the equivalent mass. To get the equivalent mass of the elastomer, the actuator is considered to be composed of n elements that are evenly divided, as depicted in Figure 3.7. Because each q_{th} element has its own displacement $x_q = \Sigma_{i=1}^{q} dx_i$, and acceleration $\ddot{x}_q = \Sigma_{i=1}^{q} \frac{d^2 x_i}{dt^2}$, assuming that $m_i = dm = (\rho\Lambda)/n$ and $d\ \ddot{x} = \ddot{x}/n$, the inertial force term will be

$$M_L \ddot{x} = dm[nd\ddot{x}_1 + (n-1)d\ddot{x}_2 + \cdots + \ddot{x}_n] = \frac{(n+1)}{2n}\rho\Lambda_L \ddot{x} \tag{3.8}$$

where ρ is the mass density of the elastomer, Λ_L is the volume, and M_L denotes the equivalent mass of the left half of the actuator. Similarly, a model of the right half of the actuator can be derived. The overall equivalent mass of the elastomer becomes

$$M = M_L + M_R = \frac{1}{2} \cdot \rho \cdot \Lambda \tag{3.9}$$

where Λ denotes the total volume of the elastomer and M_R means the equivalent mass of the right half of the elastomer. Because elastomers are viscoelastic materials, they have complicated energy dissipating mechanisms. Therefore, it is not easy to take all the effects into consideration for modeling. Instead, overall effects had better be included in the model by introducing the concept of equivalent damping, which may not be constant but in the form of an equation.

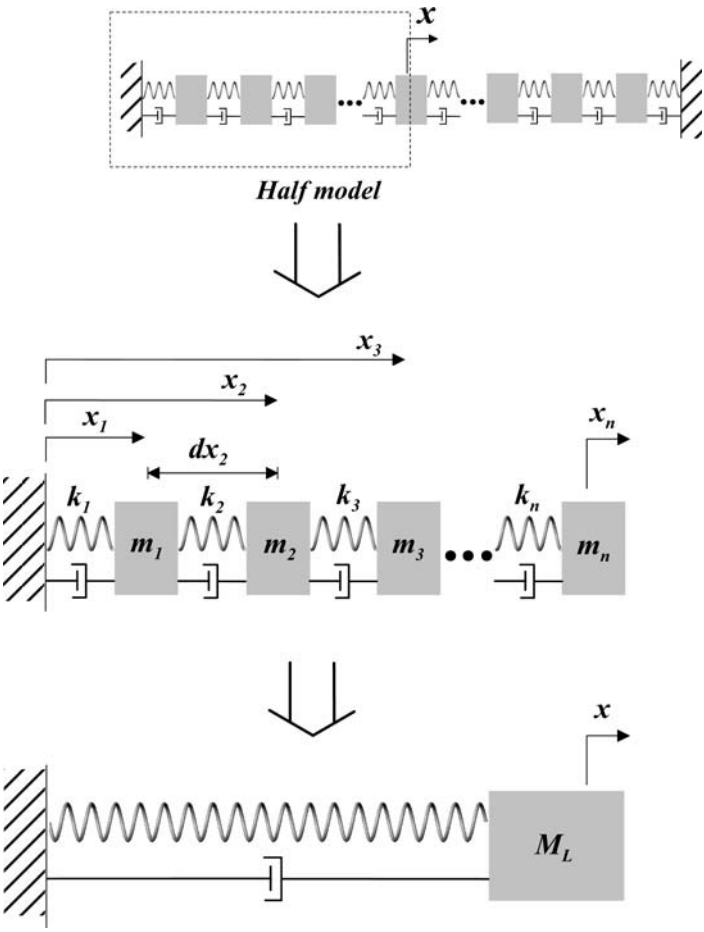

Figure 3.7. Lumped mass model for left half of actuator

For example, the equivalent viscous damping $B(\dot{x})$ of VHB4905 can be represented as

$$B(\dot{x}) = \frac{h}{\omega^{0.25}} \dot{x}^{1/2} \tag{3.10}$$

where h denotes the hysteretic damping coefficient of VHB4905 and ω represents the driving frequency. The h depends on the material, and it is 0.3 for VHB4905 with 200% prestrain. In the dynamic equation of Eq. (3.7), all terms are to be derived with Eqs. (3.5), (3.6), (3.9), and (3.10). This model will be useful for developing a control method for the actuator presented.

3.2.4 Control of Actuator

In this section, a method for control of both displacement and compliance of the antagonistically configured actuator is explained. For reasonable handling of the nonlinear characteristics of the actuator, a linearization of the actuator system is performed, and a modified nonlinear decoupling control method is applied to the linearized system.

3.2.4.1 Linearized System Model
From Eqs. (3.4) - (3.6), the stiffness of the actuator is calculated as

$$\kappa = \frac{\partial F}{\partial x} = \frac{\partial}{\partial x}\left[g_k K(x) - g_e E(x, V_L, V_R)\right] \tag{3.11}$$

where κ denotes the stiffness. To control the compliance of the actuator, it is necessary to find the inverse function of Eq. (3.11). It is not easy to derive a closed form solution of the inverse because Eq. (3.11) has some complicated nonlinear terms. Therefore, a linearization about the equilibrium position is needed to elaborate the inverse solution and the control law. By employing Taylor's series expansion (limited to the first order), a linearized model for the overall system is obtained as follows:

$$F = \left(-\frac{\partial P_L}{\partial x}\Big|_{x=0} + \frac{\partial P_R}{\partial x}\Big|_{x=0} \right) x + \left(-P_L\Big|_{x=0} + P_R\Big|_{x=0} \right) \overset{\Delta}{=} \kappa x + \beta \tag{3.12}$$

where κ and β mean the stiffness and the output force at the equilibrium point of the whole system. The left and right halves of the actuator are symmetrical with respect to the $x-y$ plane, so linearized equations can be derived such as

$$\kappa = A_1 - A_2\left[\frac{V_R^2}{\left(A_3 - A_4 V_R^2\right)^2} + \frac{V_L^2}{\left(A_3 - A_4 V_L^2\right)^2} \right] \tag{3.13}$$

and

$$\beta = A_5\left(\frac{1}{A_3 - A_4 V_R^2} - \frac{1}{A_3 - A_4 V_L^2} \right) \tag{3.14}$$

where

$$
\begin{aligned}
A_1 &= g_\kappa \frac{2Y_x \delta_{zp} L_{yp}}{\delta_{xp}} \\
A_2 &= g_e \frac{3Y_x Y_z \delta_{zp}^4 L_{yp} \delta_{z0} \varepsilon_o \varepsilon_r}{\delta_{x0}} \\
A_3 &= Y_z \delta_{zp}^3 \\
A_4 &= \delta_{z0} \varepsilon_o \varepsilon_r \\
A_5 &= g_e \frac{Y_x Y_z \delta_{zp}^4 L_{yp} \delta_{xp}}{\delta_{x0}}
\end{aligned}
\tag{3.15}
$$

3.2.4.2 Modified Nonlinear Decoupling Control System

By using the linearized system model, a modified nonlinear decoupling controller is developed. The controller employs a plain scheme popularly used in various control and robotic applications. It provides the ability to control both position and stiffness. Figure 3.8 shows the overall structure of the controller.

A detailed internal structure of the compliance controller that is a subpart of the controller shown in Figure 3.8 is provided in Figure 3.9. The controller is composed of an inverse equation and a stiffness compensator. Shown in Figure 3.9, the inputs of the controller are the load F, the desired stiffness k_d, and the displacement x. The outputs of the controller are V_L and V_R. Note that the stiffness k_d is the desired stiffness, and Eq. (3.12) is reconstructed as follows:

$$
\begin{aligned}
\kappa &= k_d \\
\beta &= F - k_d x
\end{aligned}
\tag{3.16}
$$

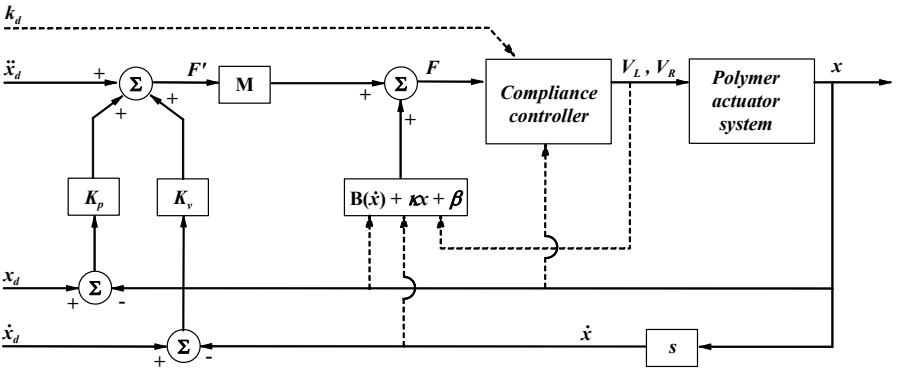

Figure 3.8. Structure of modified nonlinear decoupling controller

Therefore, the inverse solution for the stiffness input can be obtained by solving the two equations in Eq (3.16).

The input voltages are calculated by

$$V_L = \sqrt{\frac{C_1 + C_2}{C_3 - C_4}}$$

$$V_R = \sqrt{\frac{C_1 + C_2}{C_3 + C_4}} \tag{3.17}$$

where

$$C_1 = A_3 A_4^2 A_5^2 (k_d - A_1) + A_2 A_3^2 A_4 (F - k_d x)^2 - A_2 A_4 A_5^2$$

$$C_2 = \left[-2A_2 A_3 A_4^3 A_5^4 (k_d - A_1) - A_2^2 A_3^2 A_4^2 A_5^2 (F - k_d x)^2 + A_2^2 A_4^2 A_5^4 \right]^{\frac{1}{2}}$$

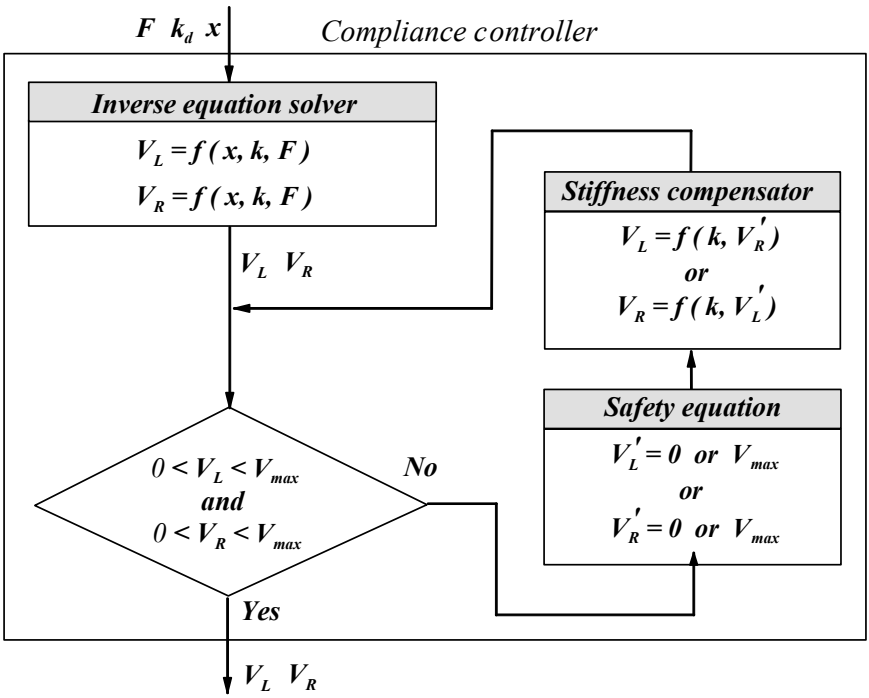

Figure 3.9. Details of compliance controller

$$C_3 = A_4^3 A_5^2 (k_d - A_1) + A_2 A_3 A_4^2 (F - k_d x)^2$$

$$C_4 = A_2 A_4^2 A_5 (F - k_d x) \tag{3.18}$$

As shown in Figure 3.9, the inverse outputs V_L and V_R obtained must be determined within the limit of the actuating voltages. Consequently, the stiffness compensator can be derived from Eq. (3.13) as follows:

$$V_L = \sqrt{\frac{-A_2 + A_3 G_R + \sqrt{A_2^2 - 2A_2 A_3 G_R}}{A_4 G_R}}$$

$$V_R = \sqrt{\frac{-A_2 + A_3 G_L + \sqrt{A_2^2 - 2A_2 A_3 G_L}}{A_4 G_L}} \tag{3.19}$$

where

$$G_L = 2A_4\left[k_d - A_1 + A_2 \frac{V_L'^2}{(A_3 - A_4 V_L'^2)^2}\right]$$

$$G_R = 2A_4\left[k_d - A_1 + A_2 \frac{V_R'^2}{(A_3 - A_4 V_R'^2)^2}\right] \tag{3.20}$$

Thus, Eq (3.17) can be termed an inverse stiffness solution.

3.2.5 Inchworm Microrobot Using Prestrained Actuator

The design of ANTLA can be directly applied to biomimetic microrobots. Some examples are shown in this section.

Annelid animals such as earthworms or maw worms, etc., contain metameric structures composed of numerous ringlike segments. In their movements, annelid animals use longitudinal muscles as well as circular ones and carry out locomotion by contracting these muscles alternatively without looping their metameric structures. To reproduce this muscle combination, three ANTLAs embedded in the metameric structure of the robot provide actuation forces, while they play the role of the frame as well. It not only enables efficient actuation but also makes it possible to manufacture a robot by a totally new fabrication method that enables mass production of a robot through processes such as injection molding or stamping [10,11]. In addition, there are possibilities to easily mimic the natural and delicate motions such as animal skin motions, wrinkling, and eyebrow movement without using many actuators. The design of the segment addressed in this section illustrates a realization of embedding actuators in the robot without using complicated mechanisms or their substitutes.

3.2.5.1 Design of a Segment

The metameric structure of annelid animals features a number of ringlike segments. The segment can be regarded as an independent actuator capable of exerting multiple DOFs of motion. As shown in Figure 3.10, the segment is composed of two parts, a lower body and the upper body. The outer diameter of the segment is 30 mm and the length is 18 mm. The lower body is composed of a plastic frame

and three ANTLAs. The ANTLAs are fixed equidistantly along the circumferential direction on the frame. The actuators are attached to the frame of the segment body made with plastics, so there is a large cavity in the central part of the segment that can be used for embedding devices and equipment that a robot has to carry for its main missions. The lower body plays a role as a connector that contains a mechanical joint and a structure for attaching another adjacent segment.

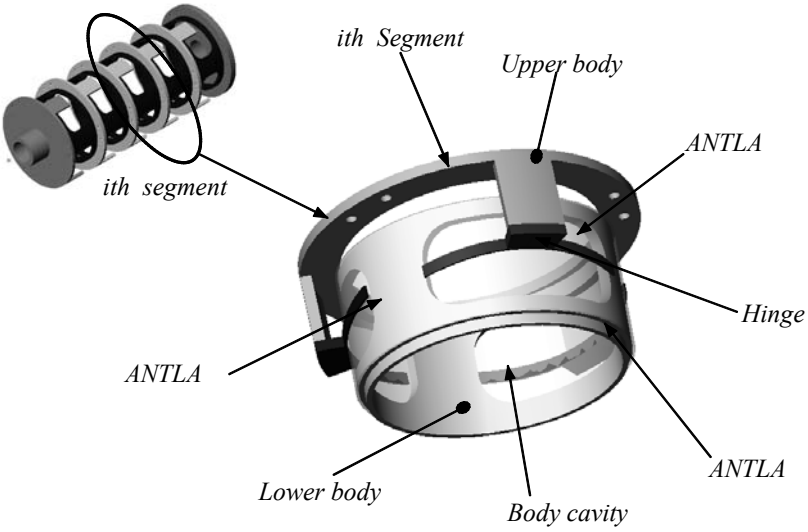

Figure 3.10. Schematic structure of a segment

Each ANTLA generates a single degree-of-freedom linear motion, so a segment composed of three of them produces three-degrees-of freedom motion. Actuation of the three actuators produces motion of the upper body relative to the lower body, thus motions like translation, panning, and tilting are possible. A segment can be modeled as a parallel mechanism with three linear actuators. The push-pull motion of the ANTLA is represented as a couple of active prismatic joints so are connectors between the upper and the lower body simplified as spherical joints.

In Figure 3.11, the motion of a segment is illustrated. The moving direction of the segment is designated with an arrow. As illustrated in Figures 3.11c and b, the segment moves up or down when all of the actuators (ANTLA) go up or down simultaneously. On the contrary, the segment turns if one ANTLA moves upward and the others go downward, as shown in Figure 3.11d. Consequently, the segment can generate three DOF motions.

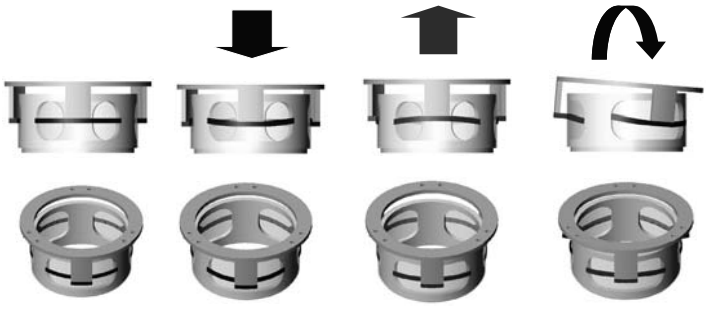

Figure 3.11. Actuating sequences of segment illustrated: (a) neutral state (b) moving upward (c) moving downward (d) turning by asymmetrical actuation

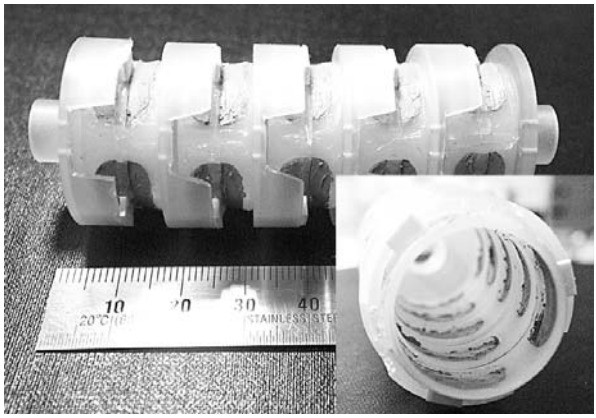

Figure 3.12. Prototype of robot and view of inside (lower right corner)

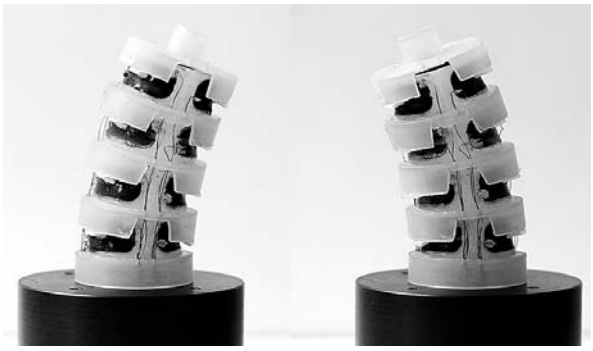

Figure 3.13. Bending motion of robot in right and left turning

3.2.5.2 A Microrobot

By connecting several segments in series, an inchworm microrobot can be created, as shown in Figure 3.12. The microrobot can generate multiple DOF motions with five segments (or can be extended to a hyperredundant one if the number of segments is increased). The robot has plenty of hollow space inside that provides a morphological structure similar to an annelid as well as a space for accommodating electronic parts, power supply, electrical wiring, and control systems for the robot operation.

An accumulated turning angle of each segment generates a bending motion of the robot, as shown in Figure 3.13. By a proper combination of sequential motion of each segment, the microrobot generates translational motion, as illustrated in Figure 3.14. The shaded region in the figure represents an active segment. First, the front segment of the actuator expands while the others remain still. Then, the next actuator expands while the front segment contracts. By a consecutive motion of the aforementioned actuation pattern from the front to the tail, the robot moves forward. A demonstration of the robot motion for translational movement in a tube is shown in Figure 3.15.

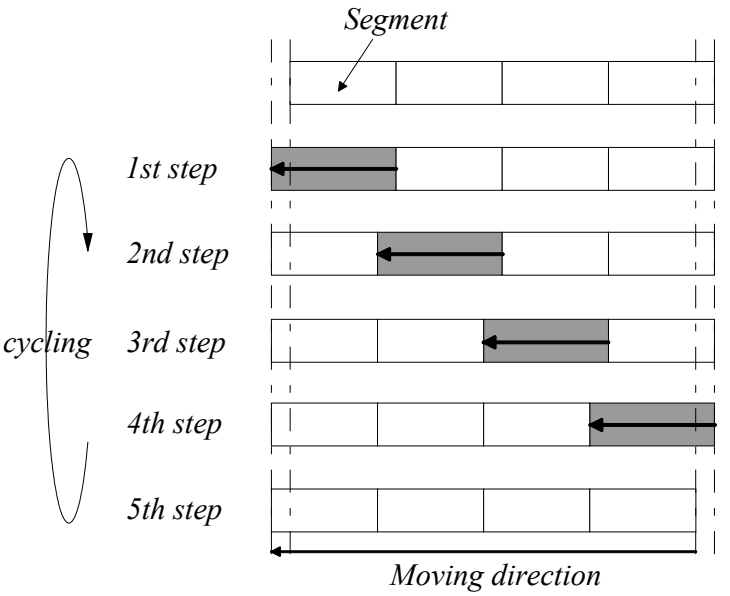

Figure 3.14. Moving sequences of an inchworm robot

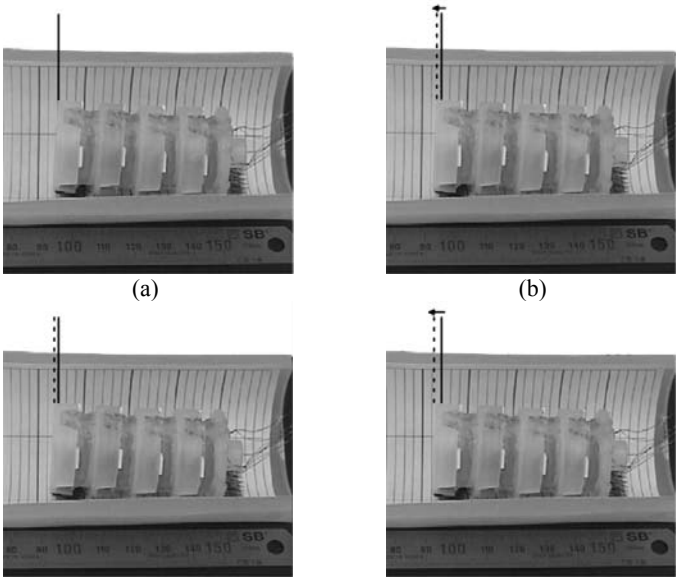

Figure 3.15. Translational motion of a microrobot (solid line: initial, dotted line: moved position)

3.2.6 Multi-DOF Linear Motor Using a Prestrained Actuator

In the previous sections, the basic working principles, benefits, and drawbacks of an antagonistically configured dielectric elastomer actuator have been delineated. Given the material and the geometrical constraints which should be well accounted for by controllable actuation of the material, the prestrained ANTLA successfully provides controlled bidirectional linear mechanical motions by changing its compliance and exerting force. Guaranteed controllability of motion with a simple control law is, of course, one of the most important design requirements of any kind of actuator. Especially, when they are applied to human-muscle like motion generators, simple architecture and easy control should be ensured.

One of the significant drawbacks of the simple ANTLA design is fragility of the film by direct external forces normal to its surface. Recognizing the disadvantages of the simple ANTLA design, a new actuator concept using dual films is introduced so that it successfully bears heavy transverse forces. This design provides a rugged linear actuation mechanism as well as expandability to multi-degree-of-freedom actuation. Furthermore, the new design is not limited to dielectric elastomer but can be directly applied to other types of polymeric actuators.

3.2.6.1 Single DOF Linear Motor

The actuator is constructed with two films made from a dielectric elastomer. A schematic of the design concept is provided in Figure 3.16.

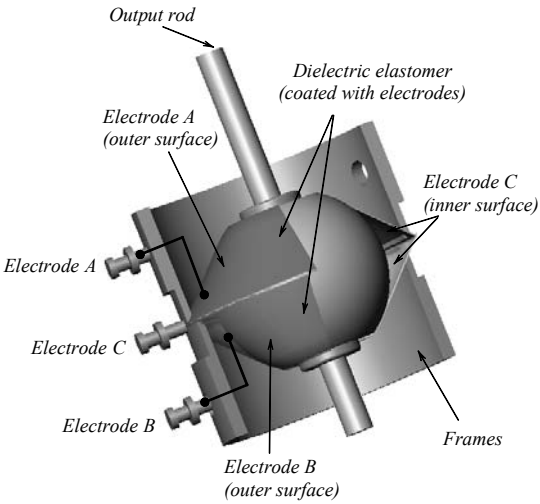

Figure 3.16. Schematic view of linear motor actuator concept

Two sheets of elastomer film are used for the design. Each film is mounted on a circular frame that works as a ground electrode. It is designated electrode C in the figure. The two mounted films are prestrained by sandwiching a pretensioning rod. Once the assembly is done, the rod is positioned and remains at the strain force equilibrium of the two pretensioned elastomer units unless electrical input is applied. If the elastic force equilibrium is broken for any reason, the rod will move either upward or downward and stops at a new equilibrium position. This is the fundamental working mechanism of the actuator.

A more detailed explanation of the actuator working mechanism is provided in Figure 3.17. When an electric potential is applied to electrodes A and C across the top film, the dielectric elastomer film expands, and it results in breaking the initial strain force balance.

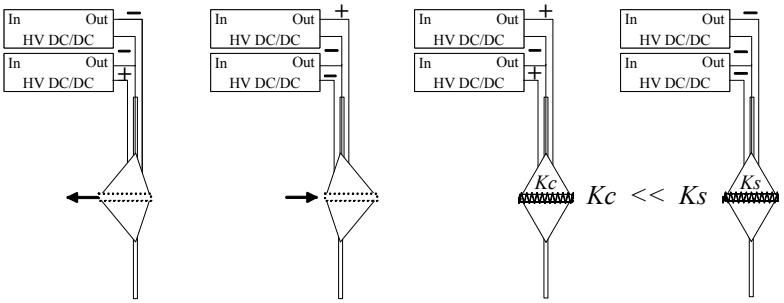

Figure 3.17. Principal actuation mode

Hence, the rod will move upward and stop at a new equilibrium position. Because both polymer films are constrained by each other through the rod, the proposed actuator motion should be controllable only by adjusting the stiffness of the films.

The actuator is to return to its original state as soon as the input is removed, and the actuation can be, of course, easily reversed by applying electrical input to the bottom film. Similarly, a push-pull actuation is possible by alternating actuations of the two. Some example patterns of actuator driving are listed in Table 1. This paradigm provides four distinct working modes, forward, backward, highly compliant, and highly stiff, those are similar to human muscle fibers.

Having controllability of the linear actuator introduced, a single-DOF linear actuator is constructed, named a *polymer motor*. A schematic cross-sectional view of a fully packaged motor assembly is shown in Figure 3.18.

Table 3.1. Linear motor driving paradigm

State	Electrode (ABC)						
Stiff state	-	-	-	or	+	+	+
More compliant	+	+	-	or	-	-	+
Action toward A	+	-	-	or	-	+	+
Action toward B	-	-	+	or	+	+	-

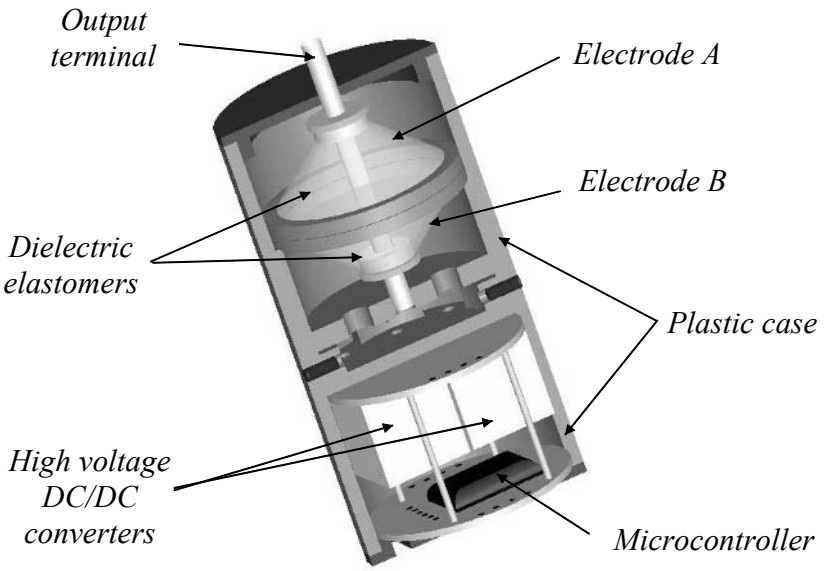

Figure 3.18. Cross-sectional view of polymer motor

The thrust force and physical size of the actuator are potentially scalable so that it could be applied for various actuator operations ranging from microrobotics to consumer electronics. Moreover, it generates a thrust force by a true linear mechanism without any mechanical transformers, which guarantees higher energy efficiency, quiet operation, and easy control. A prototype of the polymer motor is

shown in Figure 3.19. All of the essential components such as the dielectric elastomer actuator, the driving circuits, the microcontroller, and an RS-232C serial interface are integrated in a unit.

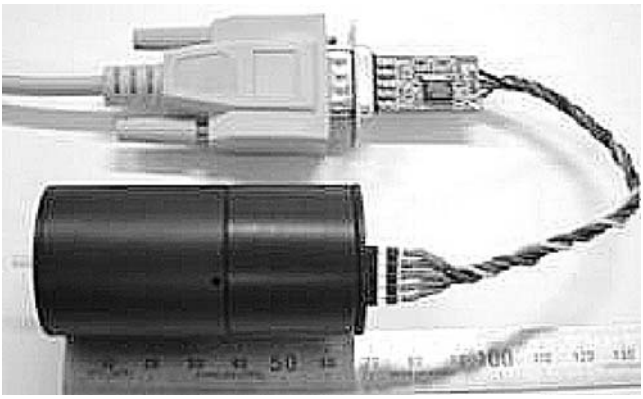

Figure 3.19. Prototype of polymer motor

3.2.6.2 Multi-DOF Polymer Motor

The concept presented of the single-DOF polymer motor can be easily extended to a multi-DOF motion actuator using a partitioned electrode coating scheme that is illustrated in Figure 3.20. The actuator consists of eight polymer film sections, four sections on each side. It could be manufactured by simply partitioning the elastomer surface and applying the carbon coating separately on each partitioned area during the electrode coating process. Each polymer section is divided with separate electrodes, so each quadrant must be controlled independently.

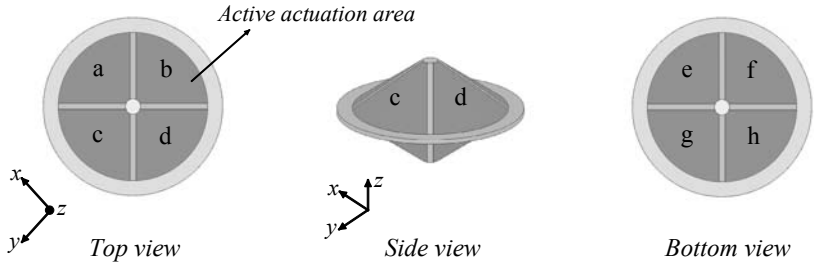

Figure 3.20. Schematic of a five DOF polymer motor design

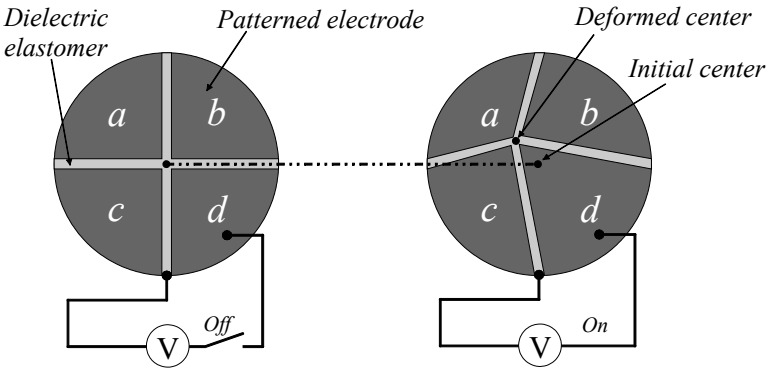

Figure 3.21. Generation of multi-DOF motions

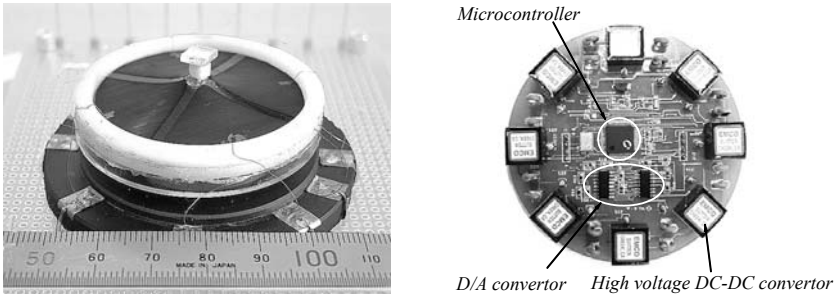

(a) actuator body (b) driving circuitry

Figure 3.22. Prototype of a five DOF polymer motor

A proper combination of individual motions of each section might provide continuous multi-DOF actuation. For example, when sections *d* and *h* are actuated, the output terminal moves in the positive *x* direction. Figure 3.21 shows the generic idea for creating translational motions. If sections *c* and *f* are turned on in a non-symmetrical input pattern, the output terminal will be tilted with respect to the positive *x* axis. Then, if the control action succeeds in providing electrical input to sections *d* and *e*, the terminal will rotate about the positive *y* axis.

Further continuous control action with proper adjustment of the input voltage during the transition of the rotating axis helps to keep the terminal in smooth rotation. A prototype of the multi-DOF polymer motor is shown in Figure 3.22 with its control circuit that could be combined in an actuator assembly.

3.3 Nonprestrained Dielectric Elastomer Actuator

3.3.1 Fundamentals of Nonprestrained Actuator

Having some amount of prestrain on dielectric elastomer actuators improves the deformation and helps in generating macromotions. However, there are a few counteractions due to the prestrain. One of the critical drawbacks is stress relaxation and hysteresis, although the extents depend on the materials, and it is still the key concern over the actuator.

Recognizing the disadvantages of prestrained actuator designs, in the following sections, a different actuator design concept without using pretension is introduced that maintains the initial performance without the rapid aging process that happens by relaxation. The stress relaxation of the prestrained actuator is illustrated in Figure 3.23. The working procedure of the actuator depicted in Figure 3.23 is (a) initial state - the restoration force of stretched actuator F_L is balanced by the restoration force of elastic body F_R such as a spring or other elastomer; (b) actuation state - a longitudinal expansion force F_m, which leads from the electrostatic force $F_{Maxwwell}$ that is engaged on the actuator in the vertical direction by applying voltage, is added to the restoration force; (c) new equilibrium state - the two materials, dielectric elastomer actuator and elastic body, are deformed to rearrange the equilibrium condition of the restoration forces.

Assuming uniform pretensions are engaged along the prestrain, the tensions on both elastomer films are initially balanced in that direction. Once the electrical input is applied that induces Maxwell stress, the balance is broken. Then, the mid point is moved by the unbalanced force, and it stops at a new balanced position. This process generates a large force and displacement.

As mentioned, however, the actuator design has a couple of drawbacks. First of all, the most significant problem is caused by the viscoelastic characteristic of polymer materials. A viscoelastic material shows a combination of elastic and viscous behavior so that an applied stress results in an instantaneous elastic strain followed by a viscous time-dependent strain.

The time-dependent behavior of the material under a quasi-static state can be categorized into three types of phenomena: creep, stress relaxation, and constant rate stressing. Figures 3.24 and 3.25 show the viscoelastic behavior of VHB4905 (3M) that is one of the most representative dielectric elastomers.

Most prestrained actuator designs suffer from viscoelastic characteristics. Hence the stress induced by the stretching of the elastomer gradually decreases and the output force of the actuator may decrease because the maximum actuation force is dependent on the pretension of the elastomer. In addition, the actuation of the pre-strained elastomer normally requires another elastic counterpart such as a spring or elastomer, as shown for ANTLA.

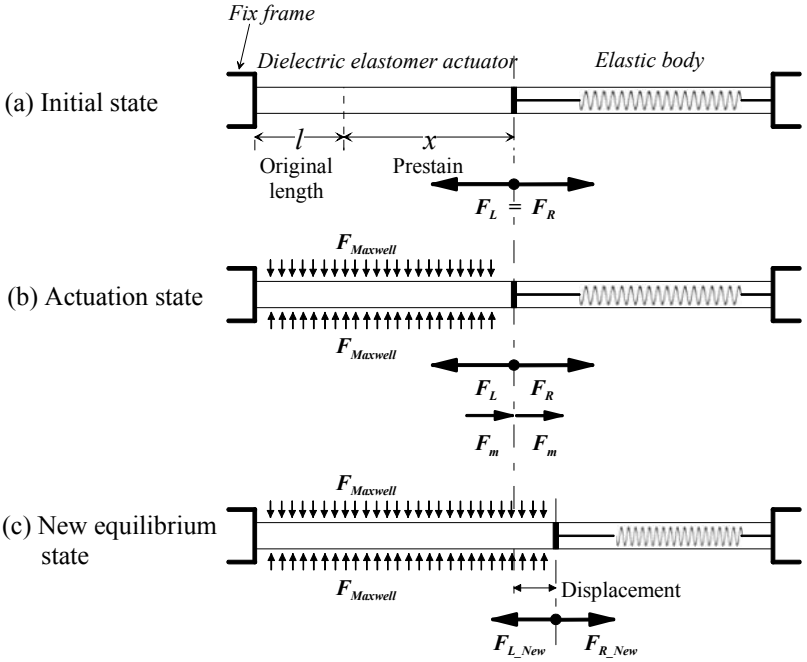

Figure 3.23. Stress relaxation

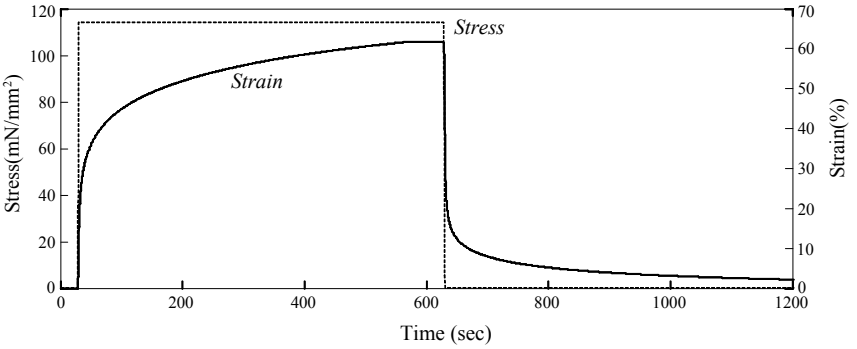

Figure 3.24. Creep at constant stress

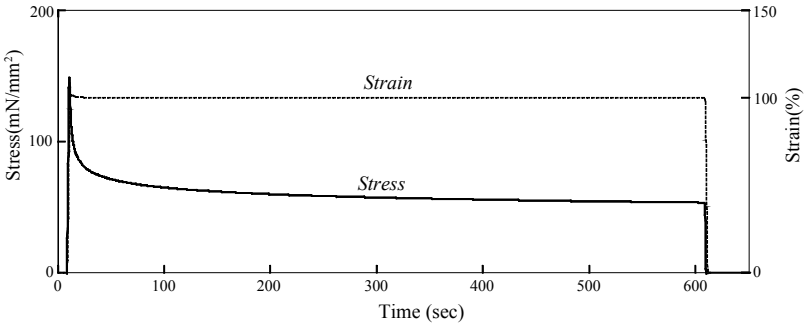

Figure 3.25. Stress relaxation at constant strain

To avoid the time-dependent behavior of the dielectric elastomer actuator, the pretension should be removed and only a pure compressive force induced by the Maxwell stress should be used for actuation. For the first step of the nonprestrained actuator design, the amount of deformation of the dielectric elastomer caused by the Maxwell stress must be calculated. The governing equation should be modified for the vertical strain δ_z according to the compression stress σ_z.

$$t = (1+\delta_z)t_0 \tag{3.21}$$

$$\frac{\sigma_z}{Y} = \delta_z = -\frac{1}{Y}\varepsilon_o\varepsilon_r\left(\frac{V}{(1+\delta_z)t_0}\right)^2 = -\frac{1}{Y}\varepsilon_o\varepsilon_r\left(\frac{V}{t_0}\right)^2\frac{1}{(1+\delta_z)^2} \tag{3.22}$$

$$\delta_z^3 + \delta_z^2 + \delta_z = -\frac{1}{Y}\varepsilon_0\varepsilon_r\left(\frac{V}{t_0}\right)^2 \tag{3.23}$$

where Y denotes the elastic modulus, δ_z is the strain in the vertical direction, and t_0 is the initial thickness.

Figure 3.26 shows the vertical strain δ_z curve versus voltage for silicone KE441(ShinEtsu) whose material properties are shown in Table 3.2. As shown in Figure 3.26, the estimated amount of compressive strain is about 1-3.5 %, although that is dependent on the material properties and the applied input voltage. Most of dielectric elastomers are incompressible, so if the actuator is assumed to be a thin circular disk, the strain is derived as

$$(1+\delta_x)(1+\delta_y)(1+\delta_z) = (1+\delta_r)^2(1+\delta_z) = 1 \tag{3.24}$$

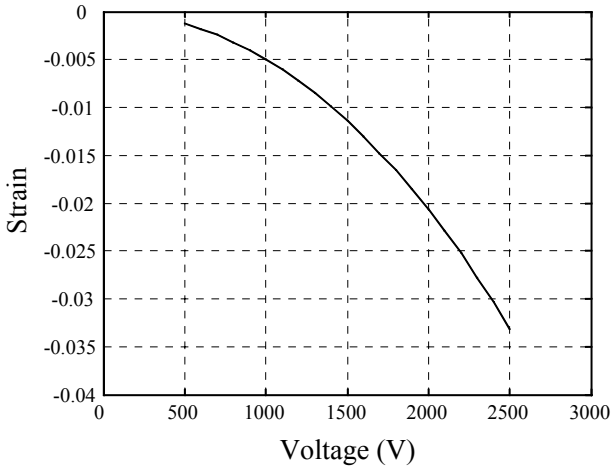

Figure 3.26. Simulated strain curve versus given voltage

Table 3.2. Material properties of KE441 silicone

Elastic modulus (Mpa)	2
Breakdown voltage (kV/mm)	20
Relative permittivity	2.8

where

$$\delta_r = 1/\sqrt{1+\delta_z} - 1 \tag{3.25}$$

Approximation of Eq. (3.25) yields

$$\delta_r \approx -(1/2)\delta_z \tag{3.26}$$

Eq. (3.26) means that the usable strain is only half of the vertical strain. For that reason, either a material with a higher dielectric constant or very high input voltage is required for a better actuator performance. However, neither seems to be very practical because the polymeric materials commercially available have limited dielectric characteristics and the electrical circuit devices handling high voltage are also limited. Therefore, a new actuating method has to be developed for the nonprestrained actuator.

The basic operating concept of the nonprestrained dielectric actuator is illustrated in Figure 3.27. As shown in Figure 3.27a, a thin dielectric elastomer sheet is confined by rigid boundaries. Once a compressive force is applied to the sheet, it must expand. That induces buckling situation in the sheet and the sheet has to become either convex or concave. This idea makes an efficient actuation without

prestrain. The relation between the curvature r, the angle θ, and the strain δ_a can be derived as follows:

$$b = a(1+\delta_a) = r\theta \tag{3.27}$$

$$r = \sin(\theta/2) = a/2 \tag{3.28}$$

$$\frac{\theta}{\sin(\theta/2)} = 2(1+\delta_a) \tag{3.29}$$

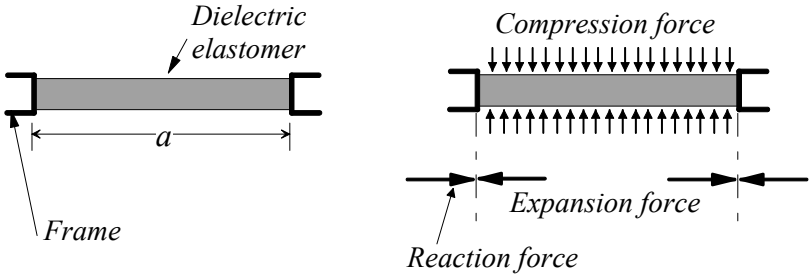

(a) initial state (b) actuated state

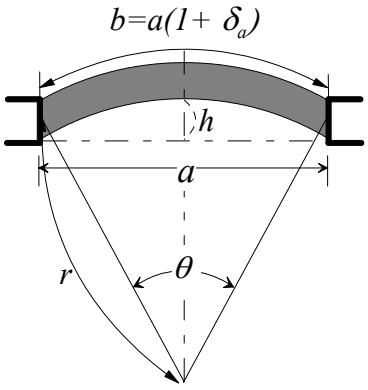

(c) deformed state

Figure 3.27. Basic operating concept of the nonprestrained actuator

From the Taylor series expansion,

$$\sin(\theta/2) \approx \left(\frac{\theta}{2}\right) - \frac{(\theta/2)^3}{3!} = \frac{\theta(24-\theta^2)}{48} \tag{3.30}$$

By substituting Eq. (3.30) in (3.29), angle θ can be derived as follows:

$$\theta = \sqrt{24[1-1/(1+\delta_a)]} \tag{3.31}$$

The strain can be derived using Eqs. (3.23), (3.24), and (3.30) so that the displacement h is

$$h = r[1-\cos(\theta/2)] \tag{3.32}$$

where

$$r = \frac{[(1+\delta_a)a]}{\theta} \tag{3.33}$$

3.3.1 Prototype Building and Testing of a Nonprestrained Actuator

3.3.1.1 Actuator Prototype

In Figure 3.28, a schematic illustration of the nonprestrained actuator construction is provided, and its actual dimensions are listed in Table 3.3. KE441(ShinEtsu) silicone that has a lower viscosity than VHB4905 is used. The spin-coated elastomer film has been coated with carbon electrodes. They are stacked to make multiple layers. The total membrane thickness is 0.75 mm and each dielectric elastomer is approximately 0.05 mm thick. To make an insulated area between electrodes, both sides of the dielectric elastomer have a nonelectrode area. The diameter of the membrane (d) is slightly larger than that (d_f) of the fixed frame and it might create either a concave or convex circular membrane that could provide more stable control of deformation in the desired direction during actuation. Figure 3.29 shows an actual fabricated prototype of a dielectric elastomer actuator.

Only the area with electrodes, d_r, expands when a driving voltage is applied; thus δ_r should be converted into δ_a that can be derived as

$$\delta_a = \delta_i + \delta_r \frac{d_r}{d} \tag{3.34}$$

Table 3.3. Dimensions of the nonprestrained actuator

d	5.8 mm	d_f	5.7 mm
d_r	5.1 mm	t	0.75 mm

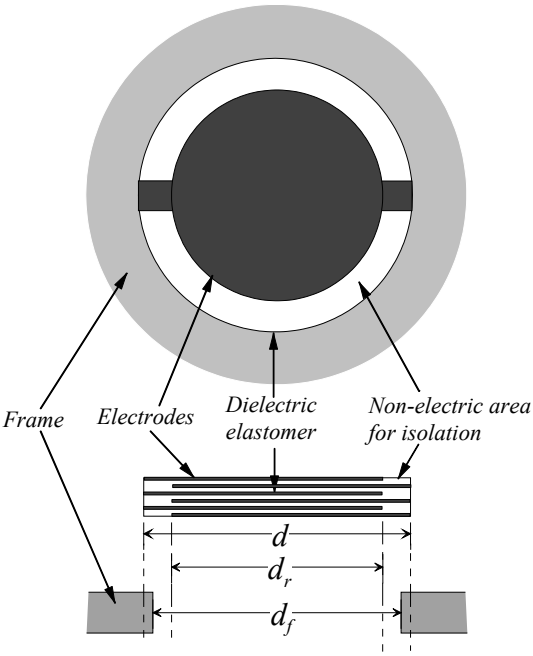

Figure 3.28. Schematic illustration of nonprestrained actuator construction

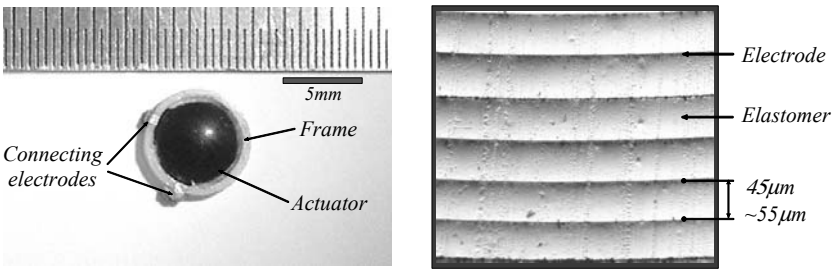

Figure 3.29. Prototype of a nonprestrained actuator

where δ_a denotes a converted strain, and δ_i is an initial strain given by the initial condition $\delta_i = \left(d / d_f - 1\right)$. δ_r is given by Eq. (3.25) and the vertical displacement h is derived by Eq. (3.32).

3.3.1.2 Driving Circuit

A schematic diagram of the driving circuit for the elastomer actuator is provided in Figure 3.30. The response and output characteristic of the actuator are closely related to the charging-discharging characteristics. The duration of the charging process depends on the physical properties of the polymer and is difficult to improve electrically, whereas the discharging duration can be reduced by adding a simple switching device, as shown in the figure. By the addition of the discharging circuit, the actuator can be operated at more than 100 Hz input frequency without significant attenuation.

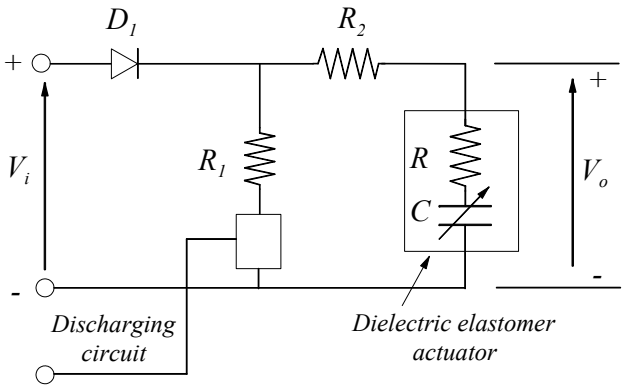

Figure 3.30. Driving circuit

3.3.1.3 Simulation and Experimental Results

A test and an analysis have been compared in Figure 3.31. The simulation and the experiments have shown good agreement. There is a small error between the calculated result and the experiment that might happen because of the disparity and difference in the thickness of each layer, the externally coated shield layer, and the fabrication process.

For complete measurement of the actuator performance, the frequency response of the actuator is also tested in both displacement and force. As shown in Figure 3.32, the soft actuator generates a fairly large displacement and force. The weight of the actuator is only 0.02 g, and its diameter is 6 mm with a 0.75 mm thickness. Besides, the actuator shows a fast response for square waveform inputs, as shown in Figure 3.33.

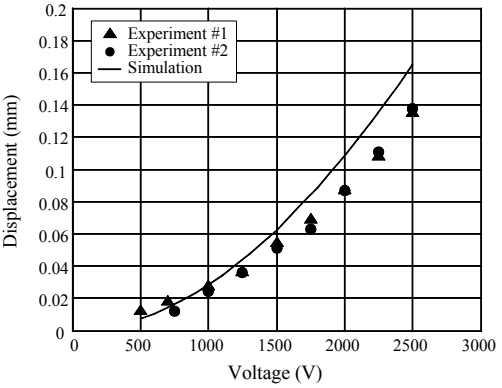

Figure 3.31. Comparison of displacement in analysis and test

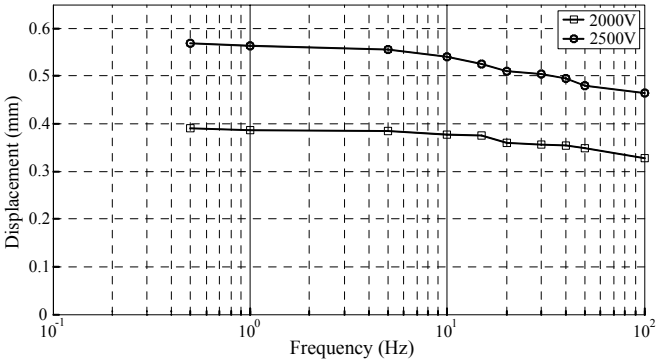

(a) displacement

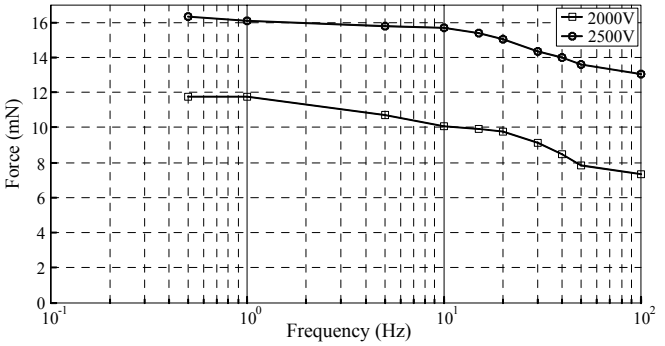

(b) force

Figure 3.32. Frequency response of a nonprestrained actuator

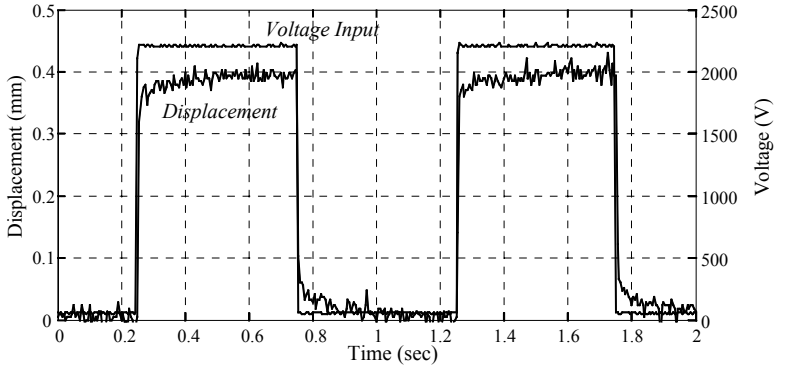

(a) displacement

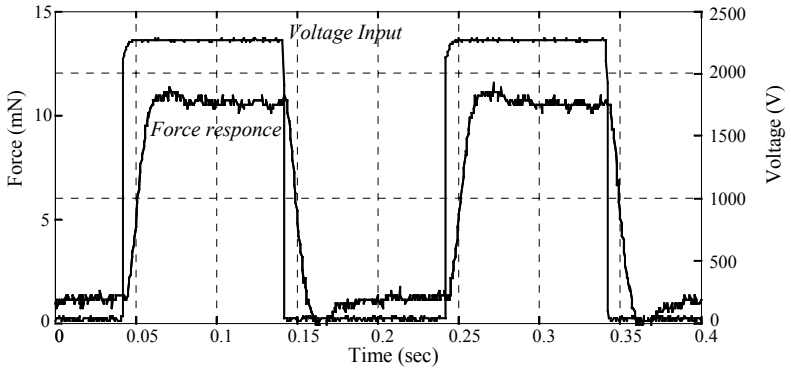

(b) force

Figure 3.33. Actuator output with square wave inputs

3.3.2 Inchworm microrobot Using a Nonprestrained Actuator

An inchworm robot made with the nonprestrained actuator has been developed as an example of actuator applications. In Figure 3.34, an actuator module that has three degrees of freedom is shown. If the module is serially connected, a multi-degree-of-freedom inchworm could be constructed. The actuator module is made with 12 serially connected modules. This actuator module works as both a power plant for the movement and a body skeleton of the inchworm robot structure. In other words, the inchworm robot can be built by simply stacking the actuator modules without any additional mechanical structure.

The actuator module shown in Figs. 3.34 has a 20mm diameter, 3mm thickness and 0.4g weight. In Figure 3.35, a fully assembled inchworm robot is shown. This robot has eight actuator modules (96 actuators). Four wires for supplying electric power are connected to the each module. For connecting each module, small silicone cylinders, which have a 1mm diameter and 0.2~0.4mm height, are used to make point-to-point connections between modules and they are bonded by silicone

adhesives. The inchworm robot is parted with front and rear sectors and each sector has four actuator modules. Each sector is operated sequentially to create inchworm motion.

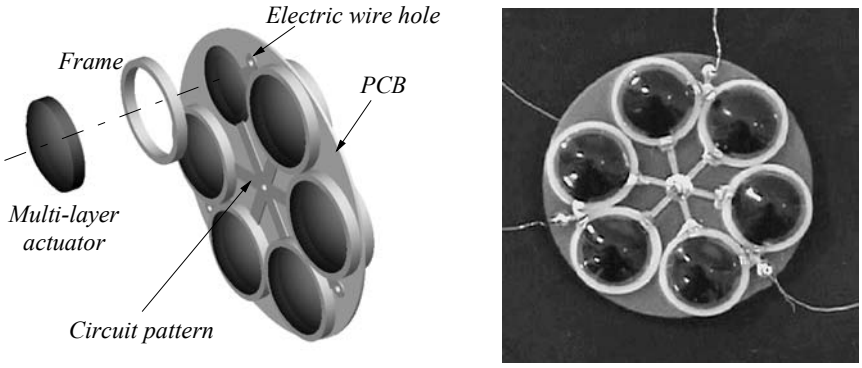

Figure 3.34. An actuator segment of nonpresetrained actutor

Figure 3.35. An inchworm robot

3.3.3 A Braille Display Using Nonpestrained Actuators

Although visual graphical display devices have been the dominant method for information interchange, the role of tactile sense is getting more attentions as a new the way of modern information exchange in various technical fields such as robotics, virtual reality, remote manipulation, rehabilitation, and medical engineering. For human-device interface application, a tactile display transfers information through controlled displacement or force that stimulates human skin.

Communications relying only on graphical presentations are definitely impossible for the visually impaired. For that reason, a large population in the world might be left out of Internet access that results in isolation from educational

resources and cultural activities. Advances in tactile display technology for higher sensitivity and higher resolution might benefit the handicapped.

Braille is a tool for exchanging information among the visually disabled and has been extensively used to transfer textual information. It consists of six pins arranged in pattern of a 3×2 matrix (a 4×2 matrix for Chinese characters). Information is delivered by stimulating fingertips by vertical displacement of the pins. The tactile display device can be used as a refreshable dynamic braille. In particular, application of the display also can be expanded to a tablet capable of displaying textural or graphical information. With that capability, even an entire web page can be delivered in a single display step. However, it is very difficult to enable braille to deliver graphical information mainly due to the limitation of arranging massive braille dots for high spatial density. The complicated and bulky driving mechanism of a conventional tactile display hampers development of high-resolution tablet type braille. According to a physiological study for standardization of braille devices, the pin-matrix density of a tactile display is typically up to one cell per square millimeter, the actuating speed should be faster than 50Hz, and the energy density must be about 10W per square centimeter [12,13]. Although the numbers are based on experimental studies, the outcome of the display function is often deceptive because the sensitivity of responses depends on testing conditions such as speed, depth, and strength of stimulation. Meanwhile various mutated tactile display types are introduced to accommodate variable human sensitivity that normally varies from fingertips to palms. Many publications introduce several different types of tactile display devices that employ pneumatics, solenoids, voice coil, shape-memory alloy, electrostatics, or electroactive polymers.

Although previous developments deserve serious attention, most of them commonly suffer from low actuation speed due to a complex actuation mechanism. Moreover, the complicated actuator design limits expansion to the tablet type application due to high manufacturing cost and low integration density. In this section, an alternative new type of dynamic braille display is introduced. Employing a dielectric elastomer as the basis of the tactile display, it is constructed with a notably simple mechanical and electrical architecture. The proposed device is organized with a dual-layered array of tactile cells, shown in Figure 3.29, which generates vertical motion to push the braille pins up or down. These electrically driven tactile cells can generate either small-scale vibratory motion or linear displacement, and they differ from the conventional devices in softness and controllable compliance, cost effectiveness, simple manufacturability, and high actuator density. Furthermore, the small size of the design introduced enables development of a high-resolution display device. Realizing the advantages of the nonprestrained actuator cell, shown in Figures 3.28 and 3.29, a braille display device has been developed using the cells. In this section, a detailed construction procedure for the device and its electronics is presented.

A typical braille display unit is constructed with six stimulating pins that are arranged in a 3×2 array format, and an array normally represents a character as defined by the Braille alphabet. The standard braille display unit is illustrated in Figure 3.36.

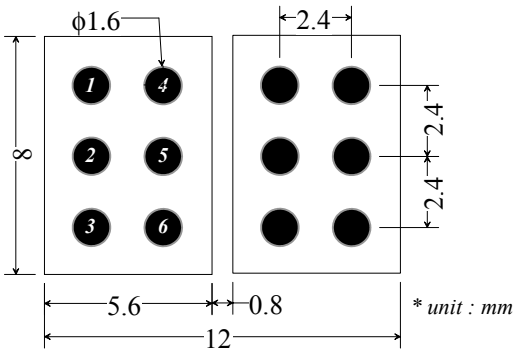

Figure 3.36. Standard braille cell consisting of six dots

In this section, a braille display unit is constructed with the introduced non-prestrained actuator tactile cells arranged in the format defined by the standard braille display.

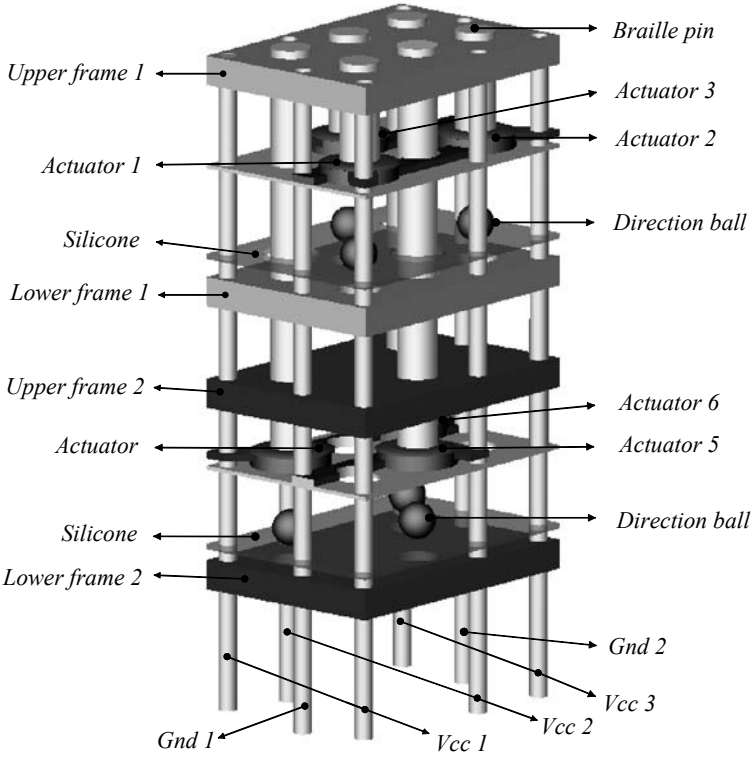

Figure 3.37. Exploded view of proposed braille display

The construction concept is depicted in Figure 3.37. Although the dielectric elastomer based tactile cell is driven with high-voltage electricity, users have no direct contact the actuator surface. A braille pin made of insulating material actually contacts with human fingertips. In addition to the predeformed convex feature of a cell, directional balls are placed underneath each cell to guarantee unidirectional actuation. Packaging the six pin actuators and corresponding electric wires in a constrained small space normally requires an expensive manufacturing process. Dual-layer construction is introduced to alleviate fabrication problems. By allocating three pins in each layer in a staggered pattern, interference caused by complicated wiring can be minimized. Each layer is shown in Figure 3.39.

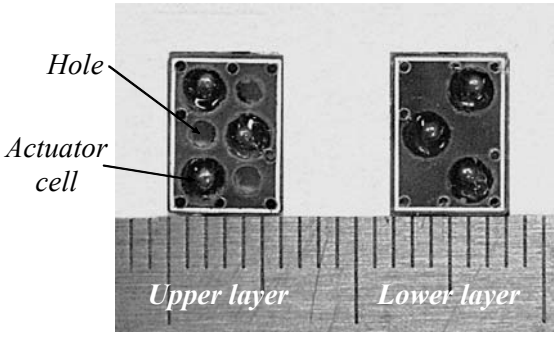

Figure 3.38. Upper and lower layers of a braille cell

As shown in Figure 3.39, the fully assembled device is only about 9mm high excluding the length of the terminals. Each braille cell is modularized for convenient installation, so each unit can be simply plugged onto a circuit board. With this simple drop-in feature, a number of braille cells can easily be combined so that a braille tablet may be manufactured by arranging many braille cells in a matrix format, as illustrated in Figure 3.40. A complete actuator system for a braille display unit composed of an embedded controller, high-voltage driving circuit, and a host PC is organized and its schematic description is provided in Figure 3.41. All necessary control electronic parts are embedded and packaged on a PCB and it communicates with a hosting PC through a universal serial bus. A microcontroller (AVR, Atmega 163) is used for the controller and USB 1.1 (Philips, PDIUSBD12) works for communication. A D/A converter (TI TLV5614) and OP-Amp (TI TLV4112) have been integrated in the controller for the modulation of high electric voltage. A complete circuit board is pictured in Figure 3.42.

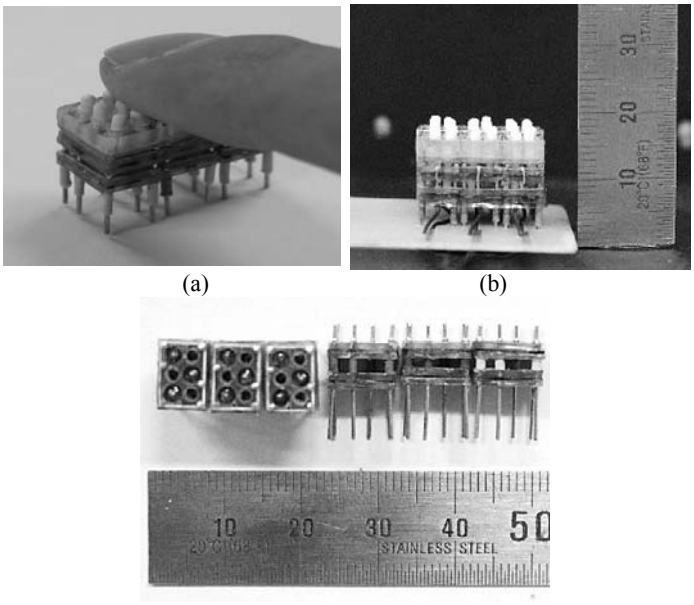

(a) (b)

(c)

Figure 3.39. Assembled braille cell

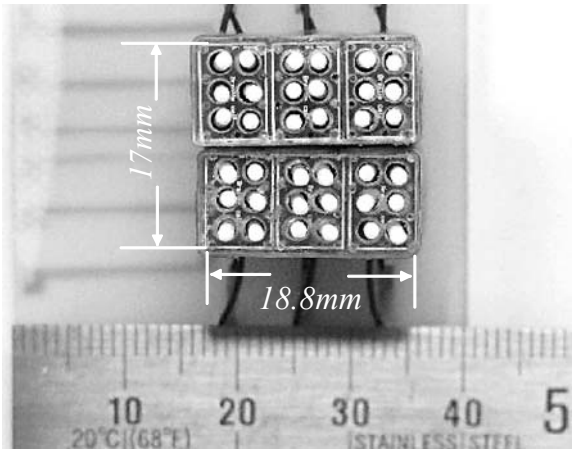

Figure 3.40. Braille tablet by assembling six modules of braille cells

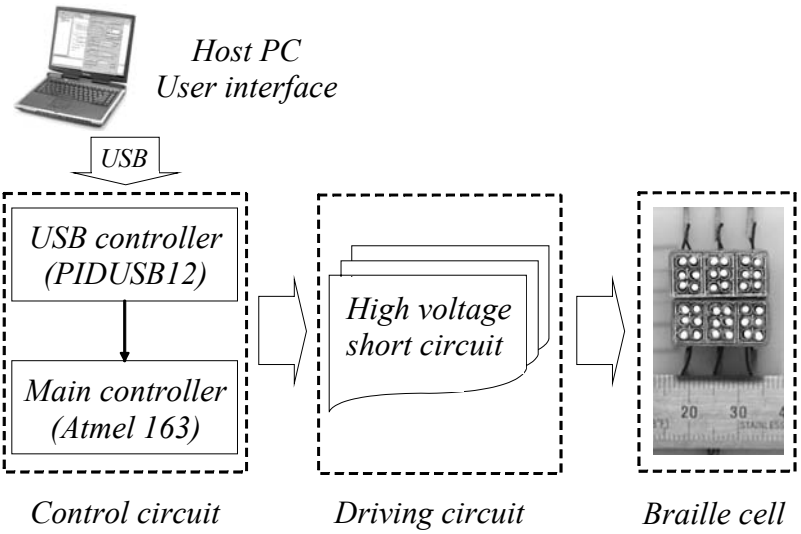

Figure 3.41. Schematic illustrations of a complete braille display unit

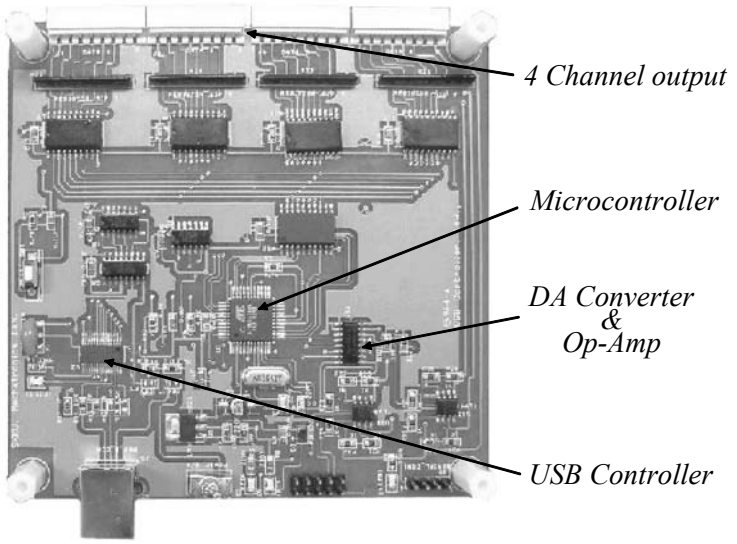

Figure 3.42. Control and communication circuit board

The device is organized by cramming many small-scale actuators into a tiny space, electrical wiring might be one of the key problems to be resolved. Identifying constructional and functional analogies of the braille device to a computer input keyboard, a control scheme, so-called dynamic scanning actuation(DSA), can be

used here. This strategy enables easy control of n×n braille cells with only 2n electrical lines. The concept of the control is depicted in Figure 3.43. One of the lines named a data line delivers high-voltage driving electric power to each cell and the other line called a scan line functions as a ground. Therefore, each actuator cell can be driven using n lines of the data line and n lines of the scan line with alternating 'On-Off' patterns on both lines.

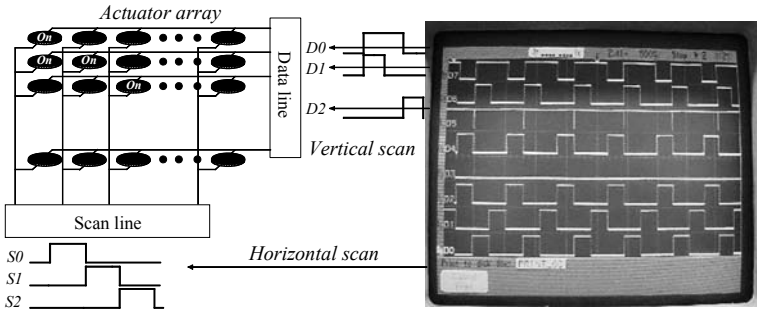

Figure 3.43. Concept of dynamic scanning actuation

For example, refer to Figure 3.43, although the data lines D0, D1, D2 get 'High'/'On' signal during three clocks, only one actuator located in the upper left corner operates because only one scan line S0 maintains 'High'/'On' during the time. In essence, an actuator cell moves only if those two lines are synchronized with a 'High'/'On' signal. The scan frequency is $\boldsymbol{L} \times \boldsymbol{M}$ when the number of actuators in a row is $\boldsymbol{M}$ and the desired driving frequency is $\boldsymbol{L}$.

Because a dielectric elastomer actuator normally operates with high electrical voltage of about 1~2kV, introduction of the proposed control scheme DSA provides significant benefits by reducing the number of required high-voltage sources. For example, a single braille unit composed of six tactile cells can be actuated with only a single voltage source, and the number of cells can be easily expanded. In Figure 3.44, HVSC (high-voltage switching circuit) high-voltage reed switches and photocouplers are shown. For faster actuator operation, the method shown in Figure 3.30 has been implemented in the circuit.

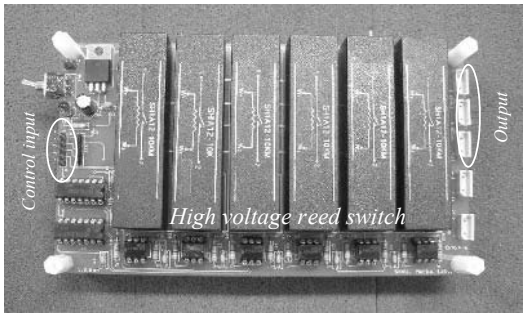

Figure 3.44. High-voltage switching circuit

3.4 Conclusions

Research and development of the dielectric elastomer actuator have produced significant progress for decades. A remarkable amount of work has focused on delivering the feasibility of the industrial application of the material. However, few commercial products equipped with polymer actuators have been introduced in the market, probably because most of the research has been dedicated either to discovering new actuation properties of the polymeric material or comparative study of the operating range of a particular traditional actuator and its polymeric substitute.

One of the implications of the term "actuator" might be a "controllable" motion generator. If a material produces just some motions, it can not be referred as an actuator unless its motions are controlled. The actuator designs introduced in this chapter have been developed under a common philosophy that actuator motions should be controllable with a reasonable amount of control actions. This clearly differs from many previous developments. The physics of the polymeric material actuation and its construction as an actuator is quite straightforward if a proper application is well sought in advance. In other words, if a good application where the polymer actuators can be used is established and the actuator functionality is well defined, application of the current dielectric elastomer actuator technology to industrial products could be accomplished before long. Future research activity may focus on development of a new energy effective material that has higher permittivity and creation of new application fields such as biomimetic robotics and tactile or braille displays.

3.5 References

[1] Y. Osaka and D. E. DeRossi (1999) *Polymer Sensors and Actuators,* Springer.

[2] Y. Bar-Cohen (2002) *Electroactive Polymers [EAP] Actuators as Artificial Muscles*, SPIE press.

[3] G. Kofod (2001) *Dielectric Elastomer Actuators*, Doctoral Dissertation, The Technical University of Denmark.

[4] R. Perline, R. Kornbluh, et al. (2000), High-Speed Electrically Actuated Elastomer with Strain Greater than 100 %, *Science*, Vol. 287, pp. 836-839.

[5] R. Perline, R. Kornbluh, and J. Joseph (1988), Electrostriction of Polymer Dielectrics with Compliant Electrodes as a Means of Actuation, *Sensors and Actuators*, Vol. 64, pp. 77-85.

[6] H. Choi, K. Jung, et al. (2005), Effect of Prestrain on Behavior of Dielectric Elastomer Actuator, *Proc. of 12th SPIE Conference*, San Diego, CA.

[7] H. R. Choi, S. M. Ryew, K. M. Jung, H. M. Kim, J. W. Jeon, J. D. Nam, R. Maeda and K. Tanie (2002), Soft Actuator for Robot Applications Based on Dielectric Elastomer : Quasi-static Analysis," *Proc. IEEE Int. Conf. on Robotics and Automation*, pp. 3212-3217.

[8] H. R. Choi, S. M. Ryew, K. M. Jung, H. M. Kim, J. W. Jeon, J. D. Nam, R. Maeda and K. Tanie (2002), Soft Actuator for Robot Applications Based on Dielectric Elastomer : Dynamic Analysis and Applications, *Proc. IEEE Int. Conf. on Robotics and Automation*, pp. 3218-3223.

[9] H. R. Choi, K. Jung, S. Ryew, Jae-Do Nam, J. Jeon, J. C. Koo, and K. Tanie (2005), Biomimetic Soft Actuator: Design, Modeling, Control, and Applications, IEEE/ASME Transactions on Mechatronics, Vol.10, No.5. pp.581-586.

[10] S. Guo, T. Fukuda, and K. Asaka (2003), A New Type of Fish-Like Underwater Microrobot, *IEEE/ASME Trans. on Mechatronics*, 8(1):136-141.

[11] M. Binnard and M. R. Cutkosky (2000), A Design by Composition Approach for Layered Manufacturing, *ASME Transactions, Journal of Mechanical Design*, Vol. 122, No. 1, pp. 91-101.

[12] N. Asamura, T. Shinohara, Y. Tojo, N. Koshida, and H. Shinoda (2001), Necessary Spatial Resolution for Realistic Tactile Feeling Display, *Proc. Int. Conf. on Robotics and Automation*, pp.1851-1856.

[13] D. G. Caldwell, N. Tsagarakis, and C. Giesler (1999), An Integrated Tactile/Shear Feedback Array for Stimulation of Finger Mechanoreceptor, *Proc. IEEE Int. Conf. on Robotics and Automation*, pp.287-292.